RSC Advances

PAPER

View Article Online
View Journal | View Issue

Cite this: *RSC Adv.*, 2022, **12**, 32526

Preparation of chitosan-coated polystyrene microspheres for the analysis of trace Pb(II) ions in salt by GF-AAS assisted with solid-phase extraction

Xingyu Ding,[a] Xin Teng,[a] Zhuxin She,[a] Yi Li, *[a] Yuanyuan Liu, *[b] Ying Zhuang[c] and Chaochao Wang[c]

Received 9th August 2022
Accepted 8th November 2022

DOI: 10.1039/d2ra04968f

rsc.li/rsc-advances

The content of heavy metals is an important index to measure the quality and safety of salt. However, due to the high content of Na(I) in salt causing a large background interference, it is difficult to accurately analyze trace Pb(II) through the existing atomic absorption spectrometry. Therefore, it is of great significance to design a new solid-phase extraction (SPE) material for the removal and determination of Pb(II) from salt. Herein, using polystyrene microspheres as carriers, the chitosan-coated polystyrene SPE fillers PS@SO_3H@G-CTS were synthesized by sulfonating with sulfonyl chloride, coating with chitosan and crosslinking with glutaraldehyde successively. The structure was characterized by elemental analysis, FT-IR, SEM, XRD and thermal stability. The SPE column prepared by PS@SO_3H@G-CTS was used for the adsorption of heavy metal Pb(II) in salt, with 0.1 mol L^{-1} of HCl as Na(I) eluent and 2 mmol L^{-1} of EDTA-2Na as Pb(II) eluent. The salt concentration below 0.03 g mL^{-1} could better reflect the performance of column, with the recovery rate of 101.17–106.45% by standard addition. The PS@SO_3H@G-CTS fillers could remove Na(I) under certain salt concentration, so as to accurately determine Pb(II) in the actual sample. Their adsorbability was undisturbed by common anions and low concentration of cations.

1. Introduction

As an indispensable condiment for daily cooking, the quality of salt directly affects human health. The contents of contaminants are an important index to measure the quality and safety of salt. The contaminants mainly refer to metals with density greater than 4.5 g cm^{-3}, including Pb, Hg, Cr, Co, Ni, Zn, Cu, Au and Ag.[1] These non-biodegradable heavy metals have a strong affinity to biological tissues, leading to their slow or complete elimination in the human body and causing progressive and irreversible damage, such as gastrointestinal and liver diseases, allergies, nerve damage, cancer and even death.[2–4] Generally, the concentration of heavy metals less than 100 mg kg^{-1} and 10 mg kg^{-1} is attributed to trace and ultra trace, respectively.[5] The Codex Alimentarius Commission (established by the Food and Agriculture Organization of the United Nations, World Health Organization and Environmental Protection Agency) with other international organizations specified the maximum permissible limit (MPL) of heavy metals in food.[6] Thus, the development of selective and sensitive analytical methods for quantifying the heavy metals at trace and ultra trace have been encouraged.[7,8] Various techniques such as inductively-coupled plasma optical emission spectrometry (ICP-OES), inductively-coupled plasma mass spectrometry (ICP-MS), graphite furnace atomic absorption spectrometry (GF-AAS), capillary electrophoresis and electrochemical detection have emerged.[9–13] Smirnova group used ICP-OES to determine Cd(II), Co(II), Cu(II), Ni(II), Pb(II) and Zn(II) in aqueous biphasic system.[9] Volzhenin group analyzed Ca(II), Pb(II) and Zn(II) in mussels by GF-AAS.[10] Lin group determined the trace Cd(II), Co(II), Cu(II), Mn(II), Ni(IV), Pb(II) and Zn(II) in water samples by HPLC and ICP-MS with the aid of chelate resins.[11] Dong group reported the electrochemical detection of Cu(II), Pb(II) and Cd(II) with UV-enhanced Ti/TiO_2 electrode.[13] Despite all this, the quantitative analysis of heavy metal ions is greatly affected by the sample matrix, and many samples need comprehensive and laborious pretreatments before instrumental analysis. This will not only increase the experimental cost, but also cause the loss and pollution of samples.

The adsorption methods have many advantages such as low cost, easy availability of materials, simple operation and high efficiency. Among numerous adsorbing materials, chitosan has wide application in heavy metals pollution remediation due to its non-toxic, easy biodegradation, environmental friendliness, low price and excellent adsorption capacity.[14–16] Chitosan is the only amino weak base polysaccharide in nature. Its molecular chains contain a large number of NH_2 and OH groups, making it chelate well with heavy and transition metals. In addition, the

[a]College of Food Science and Light Industry, Nanjing Tech University, Nanjing 211816, P. R. China. E-mail: liynj2012@njtech.edu.cn
[b]School of Pharmaceutical and Chemical Engineering, ChengXian College, Southeast University, Nanjing 210088, P. R. China. E-mail: liuyuanyuan1985419@163.com
[c]Nanjing Station of National Light Industry Food Quality Supervision and Inspection, Nanjing 211816, P. R. China

NH_2 and OH groups can form cage-like molecules with the aid of hydrogen bond and ionic bond. However, as an amorphous and translucent powder, it is difficult to recover. Recently, the magnetic chitosan polymeric materials with globular structure have attracted great attention due to its high efficiency, simple separation and easy recyclability.[17,18] Some magnetic chitosan microspheres for removing heavy metal Pb(II), Cu(II), Cd(II) and Ni(II) in water have been reported.[19–21] However, the removal and determination of heavy metals from salt are more complicated and difficult as compared to water.

As the main component of salt, sodium chloride, affected by it, the trace heavy metals in salt cannot be determined directly, and instrument such as the graphite tube of graphite furnace atomic absorption photometer may be damaged.[22,23] High salt background will accelerate the loss of graphite tube, resulting in unnecessary waste of resources and economic losses. So it is necessary to add the preseparation and enrichment before the instrumental analysis. The SPE plays an important role in sample pretreatment due to its high efficiency and convenience.[24–26] As a low-cost material, polystyrene (PS) microspheres with large surface area, strong modifiability and adsorbability have extensive application in biosensor, enzyme immobilization and chromatographic separation.[27–29] Through chemical modification of PS microspheres, our group has reported several solid-phase fluorescent sensors for rapid detection of Hg(II) in food sample.[30–33] According to the color change of microspheres, the visual recognition can be realized. Elution by EDTA or Na_2S, the regeneration of sensors can be achieved. The method is high sensitivity and selectivity, low cost, green economy and environmentally-friendly.

Due to the ultra-high content of Na(I) in salt, it is difficult to analyze trace Pb(II) by the existing atomic absorption due to its great background interference which cannot ensure accuracy. In order to design a novel SPE material for treating Pb(II) from salt with lower cost and higher efficiency, in this work, the chitosan-coated polystyrene SPE fillers PS@SO_3H@G-CTS were prepared by surface modification of PS microspheres (Scheme 1). The structural characteristics as well as properties including adsorption, separability, anti-interference and recyclability for Pb(II) were explored and discussed in details. The SPE column prepared by PS@SO_3H@G-CTS was used to pretreat the salt to reduce the background interference of Na(I) and improve the accuracy of atomic absorption analysis.

2. Experimental

2.1 Materials and reagents

Polystyrene microspheres (60 μm) were purchased from Wuxi Zhiyi Microsphere Technology Co., Ltd. Lead nitrate solution (1 g L^{-1}) was got from Tanmo quality inspection national standard material centre. Chitosan (deacetylation degree 90%, 100–200 MPa s) was bought from Shanghai Yuanye Bio-Technology Co., Ltd. Mixed strong cation (MCX) SPE column (60 μm, 60 mg/3 mL) was purchased from waters, USA. All the other reagents were of analytic grade and obtained from Nanjing Wanqing Chemical Glass Ware & Instrument Co., Ltd or Shanghai Aladdin Biochemical Technology Co., Ltd.

Elemental analyses were carried out on a Elemantar Vario EL cube. Powder X-ray diffraction (XRD) analyses were conducted on a Malvern Panalytical X'Pert3 Powder diffractometer with Cu Kα radiation, scanning from 5° to 90°. Scanning electron micrographs (SEM) were obtained by a Zeiss Sigma 300 scanning electron microscope. Fourier transform infrared spectroscopy (FT-IR) were recorded in KBr disk using a Thermo Nicolet 380 FT-IR spectrophotometer. Thermal analysis curves were gained from TA_SDT650 thermal analyzer with a heating rate of 10 °C min^{-1} under N_2 flow. Atomic absorption spectroscopy were performed on a PinAAcle 900Z graphite furnace atomic absorption spectrophotometer.

2.2 Preparation of chlorosulfonated PS microspheres (PS@SO_3H)

PS microspheres were eluted by ultrapure water (resistance > 18.2 MΩ cm), ethanol and tetrahydrofuran (THF) to remove the suspending agents, monomers and small molecules on the surface, which were then rinsed by ethanol and dried to constant weight in vacuum. Anhydrous PS microspheres (2.0 g) were swollen with carbon tetrachloride (20 mL) for 3 h, then chlorosulfonic acid (1.2 mL) was added with stirring. The sulphonation was terminated after 20 min at r.t. The products were filtrated, alternately rinsed by water and ethanol, then dried under vacuum to give 1.98 g of PS@SO_3H.

2.3 Preparation of chitosan-supported PS microspheres (CTS-supported PS@SO_3H)

To a solution of chitosan (1.5 g) in 30 mL 2% (v/v) acetic acid was added PS@SO_3H (1.0 g) and ultrapure water (20 mL). The

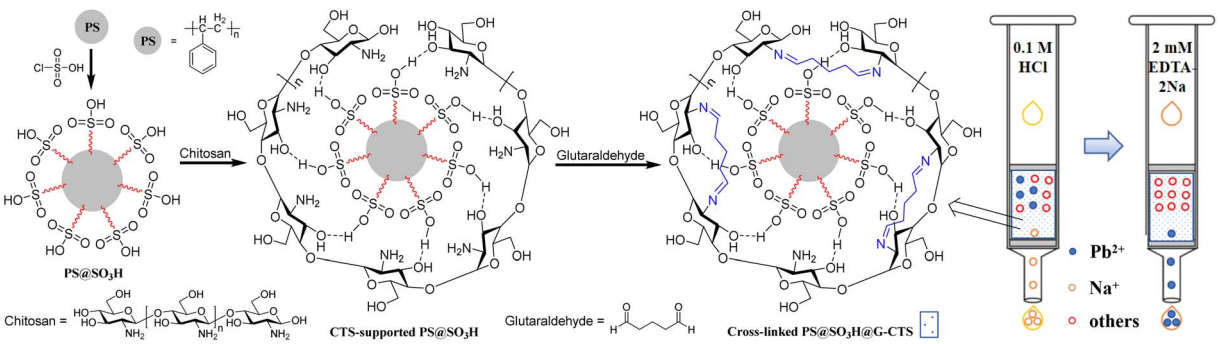

Scheme 1 Synthetic routes of polystyrene–chitosan composite microspheres.

mixture was stirred at 30 °C for 2 h, then centrifuged at 8000*g* for 5 min, dispersed with water for three times to remove the excess chitosan, then finally afforded CTS-supported PS@SO_3H (1.5 g) after rinsing repeatedly with ultrapure water.

2.4 Preparation of cross-linked chitosan-supported PS microspheres (PS@SO_3H@G-CTS)

To a suspension of CTS-supported PS@SO_3H (1.0 g) in ultrapure water (30 mL) was added 2 mL 2.5% of glutaraldehyde. The mixture was stirred at 40 °C for 2 h, then centrifuged at 8000*g* for 5 min, dispersed with water for three times, then dried under vacuum to afford PS@SO_3H@G-CTS (0.93 g).

2.5 Determination of the adsorption rate of Pb(II)

Lead nitrate solution with different concentrations of 1 μg L^{-1}, 5 μg L^{-1}, 10 μg L^{-1}, 15 μg L^{-1} and 20 μg L^{-1} were prepared. The corresponding absorbances were tested by atomic absorption to fit the standard curve.

To a centrifuge tube containing 0.001 g of PS, CTS, PS@SO_3H or PS@SO_3H@G-CTS was added lead nitrate solution (2 mL, 20 μg L^{-1}). The mixture was stood at r.t. overnight. The supernatant was separated to analyze the concentration of Pb(II) by GF-AAS and calculate the adsorption rate according to the following formula, where Ar, C_0 and C_{eq} represent the adsorption rate (%) of Pb(II), the concentration of Pb(II) (μg L^{-1}) before and after the adsorption equilibrium, respectively.

$$\mathrm{Ar} = \frac{C_0 - C_{eq}}{C_0} \times 100\%$$

2.6 Preparation and application of SPE column

A certain amount of fillers PS@SO_3H@G-CTS were loaded into an empty polypropylene tube (3 mL) with a sieve plate at the bottom (Fig. 1). Another sieve plate was pressed on the fillers for a certain time to make a small SPE column. Before use, the column was activated by 1% nitric acid and ultrapure water in turn to remove the impurities and ensure good reproducibility.

For anti-interference, four kinds of cations [Na(I), K(I), Ca(II), Mg(II)] and two kinds of anions (Cl^-, SO_4^{2-}) were added to 2 mL 20 μg L^{-1} of Pb(II) standard solution, to make the concentrations of coexisting ions from 10 to 40 g L^{-1}. The mixture was put into the column to stand overnight, then 2 mL 2 mmol L^{-1} of EDTA-2Na solution was added for elution. The eluate was collected to determine the concentration of Pb(II) by GF-AAS.

For actual sample analysis, the salt sample (5 mL) containing 20 μg L^{-1} of Pb(II) (by standard addition method) was put into the column to stay overnight. Then 10 mL 0.1 mol L^{-1} of HCl and 10 mL 2 mmol L^{-1} of EDTA-2Na were pumped into the column successively to elute Na(I) and Pb(II). The concentrations were determined by GF-AAS. The results were the average of three parallel determinations.

3. Results and discussion

3.1 Effects of chlorosulfonic acid dosage and sulfonation time on loading capacity

In order to explore the relationship between reaction time and loading capacity, the sulfonation reaction was carried out at r.t. with a molar ratio of PS microspheres to chlorosulfonic acid 1 : 1. The loading capacity increased rapidly within 5 min to 1.83 mmol g^{-1}, then changed little over time (Fig. 2). The satisfactory result was obtained when the sulfonation was conducted for 20 min.

3.2 Effects of different crosslinkers

Crosslinking of chitosan can improve its mechanical properties and reduce its solubility in acidic media. As a commonly used crosslinker, glutaraldehyde is often used as a processing aid in food industry, drug, bacteria disinfectant, tanning agent, wood preservative and polymer synthesis.[34,35] It can transform monomers, linear or pre-polymers into three-dimensional network structures under certain conditions. When glutaraldehyde acts as a crosslinker, it reacts with NH_2 on the surface of chitosan. Although it may weaken the adsorbability of chitosan, the new groups generated by crosslinking will enhance the interaction between materials and heavy metal ions, which improve the adsorption capacity. Epichlorohydrin also acts as a crosslinker, however, unlike glutaraldehyde, it reacts with the surface OH of chitosan.[36,37] In order to get the satisfactory

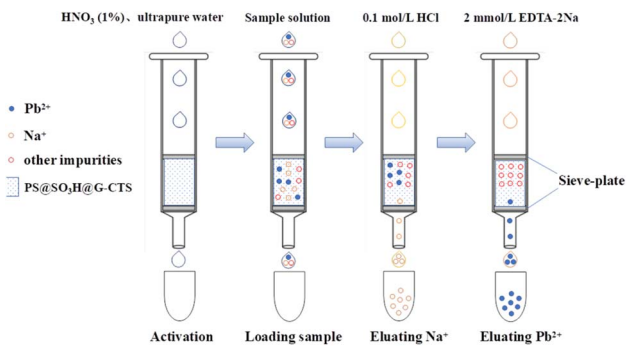

Fig. 1 The separation processes of SPE column.

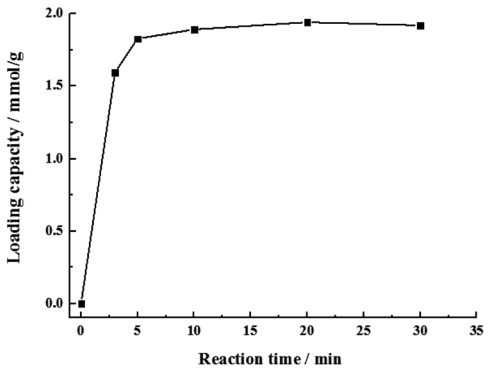

Fig. 2 The relationship between reaction time and loading capacity of sulfonation.

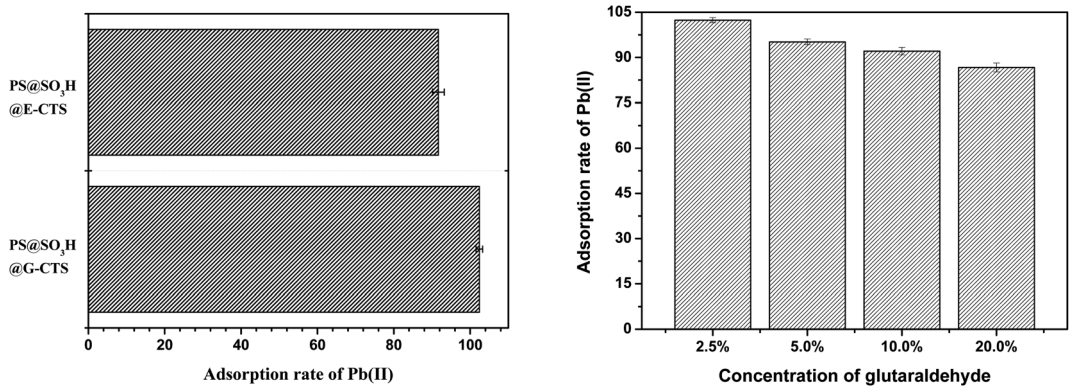

Fig. 3 Effects of different crosslinkers (left) and glutaraldehyde concentrations (right) on the adsorption of Pb(II) by chitosan modified PS microspheres.

adsorptivity for Pb(II), the crosslinking effects of glutaraldehyde and epichlorohydrin were compared in detail.

As shown in Fig. 3a, the chitosan-supported PS@SO_3H@G-CTS obtained by glutaraldehyde crosslinking exhibited stronger adsorption for Pb(II) as compared to those (PS@SO_3-H@E-CTS) obtained by epichlorohydrin crosslinking. The adsorption rate of Pb(II) based on the standard addition method was 102.41% for PS@SO_3H@G-CTS and 91.69% for PS@SO_3-H@E-CTS. Although the NH_2 decreased during glutaraldehyde crosslinking, the generated Schiff base C=N enhanced the interaction between PS@SO_3H@G-CTS and Pb(II). Although epichlorohydrin protected NH_2 during crosslinking, it also weakened its free degree, which influenced the interaction with Pb(II). So glutaraldehyde was used as the crosslinker, and the effect of its concentration on the Pb(II) adsorption of the prepared PS@SO_3H@G-CTS was explored (Fig. 3b). When the concentration of glutaraldehyde was 2.5%, the adsorption of Pb(II) was 102.41% with the least relative error. Within the range of 2.5–20.0%, the crosslinking degree increased with the increase of glutaraldehyde, resulting in the decrease of surface NH_2, which affecting its interaction with Pb(II). Therefore, PS@SO_3H@G-CTS displayed better Pb(II) adsorption with 2.5% glutaraldehyde as crosslinker.

3.3 Elemental analysis

The N and S elemental compositions of PS@SO_3H@G-CTS and PS@SO_3H were confirmed by elemental analysis (Table 1). The loaded amounts (L_A/mmol g^{-1}) were calculated by the equation below, where X and M_0 represent the mass percent and molar mass of element, respectively. The $L_{A(S)}$ in PS@SO_3H was calculated to 1.9431 mmol g^{-1}. After coating chitosan, the content of S decreased (1.8715 mmol g^{-1}) along with the increasement of N (0.0571 mmol g^{-1}) which was not found in PS microspheres, indicating the successful preparation of PS@SO_3H@G-CTS.

$$L_A = \frac{X}{M_0} \times 100\%$$

Table 1 Elemental analysis of PS@SO_3H and PS@SO_3H@G-CTS

No.	N (%)	S (%)
PS@SO_3H	0.000	6.218
PS@SO_3H@G-CTS	0.080	5.999

3.4 FT-IR analysis

The FT-IR comparisons of PS, PS@SO_3H, PS@SO_3H@G-CTS and CTS in the range of 4000–500 cm^{-1} were displayed in Fig. 4. For PS, the stretching vibrations of phenyl ring =C–H and C=C appeared at 3060, 3028, 1602, 1494 and 1450 cm^{-1}, whereas the corresponding out-of-plane bending vibrations of =C–H were found at 759 and 701 cm^{-1}. Two peaks observed at 2924 and 2851 cm^{-1} were attributed to the alkyl C–H stretching vibrations. Compared with PS, new peaks generated at 3427, 1698, 1172, 1038 and 1015 cm^{-1} in PS@SO_3H were attributed to the stretching vibration of sulfonic acid O–H and the characteristic peaks of O=S=O group. For CTS, absorption bands at 3500–3200, 2918 and 2876 cm^{-1} were attributed to the O–H, N–

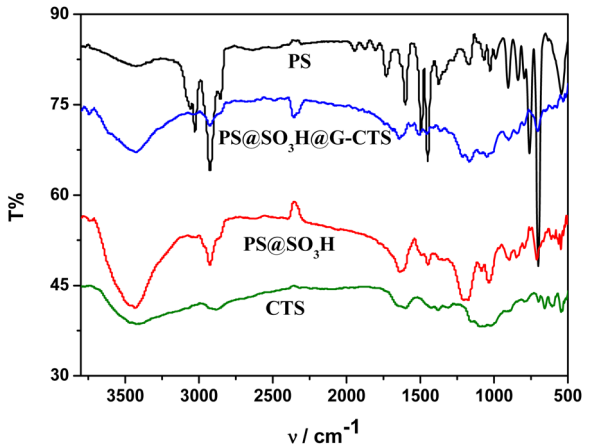

Fig. 4 FT-IR comparisons of PS, PS@SO_3H, PS@SO_3H@G-CTS and CTS.

H and C–H stretching vibrations, respectively. Three peaks found at 1375, 1153 and 1096 cm^{-1} were attributed to the out-of-plane bending vibration of O–H as well as the stretching vibrations of C–O–C and secondary alcohol. Compared with CTS and PS@SO_3H, the intensity of the similar characteristic peaks appeared in PS@SO_3H@ G-CTS weakened, which was due to the decrease of single component content after mixing the two materials. The stretching vibration of Schiff base C=N appeared at 1642 cm^{-1} along with the disappearance of chitosan O–H at 653 cm^{-1}, indicating the possible formation of new hydrogen bond between chitosan and PS@SO_3H after cross-linking. The above results indicated that chitosan were successfully coated on the PS microspheres to afford PS@SO_3-H@G-CTS.

3.5 SEM analysis

The microscopic characteristics of PS, PS@SO_3H and PS@SO_3H @G-CTS was analyzed by SEM (Fig. 5). Compared to PS (65.02 μm), PS@SO_3H had larger particle size (66.25 μm) and uneven surface, which was more suitable for the adsorption of determinand. Granular substances could be observed on the surface of PS@SO_3H, which was due to the modification of sulfo group resulting in the irregular shape of particles. After coating and crosslinking with chitosan, the zeta potential of PS@SO_3H@G-CTS composites increased with the mutual repulsion among the particles. The strong hydrophilicity of sulfo group reduced the surface tension of microspheres and led to the size decrease of PS@SO_3H@G-CTS (62.78 μm).

3.6 Thermal analysis

Thermal analysis curves of PS, PS@SO_3H and PS@SO_3H@G-CTS were displayed in Fig. 6. The PS microspheres showed the volatilization of water and residual inorganic matter under 150 °C. The decomposition temperature of the second weightlessness platform was 390 °C, indicating the polystyrene began to melt, and the exothermic peak in this range was mainly the phase transition of polystyrene. With the increase of temperature, the hot melting gradually turned into the irregular thermal de-gradation chain breaking which was maximum around 450 °C, so the exothermic peak at 450 °C was mainly the reaction heat of polystyrene. After that, the thermal weightlessness tended to be flat, especially above 500 °C, the quality of sample

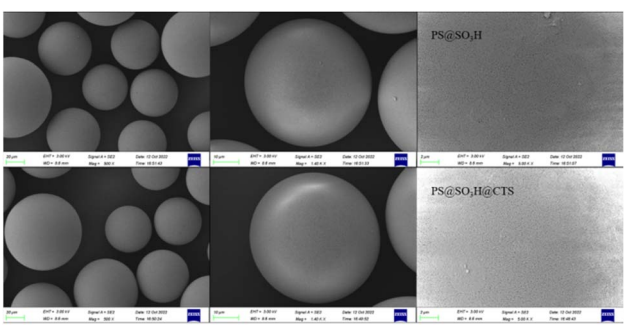

Fig. 5 SEM comparisons of PS, PS@SO_3H and PS@SO_3H@G-CTS.

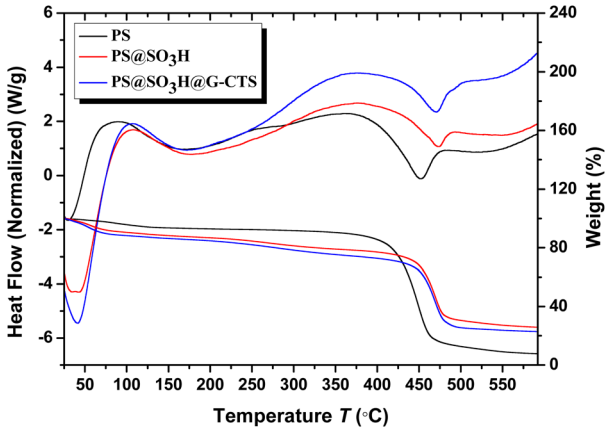

Fig. 6 TGA and DSC of PS, PS@SO_3H and PS@SO_3H@G-CTS.

hardly changed, indicating the PS microspheres have been completely decomposed. Compared with PS, PS@SO_3H and PS@SO_3H@G-CTS had three obvious weightlessness stages, and the weight loss of PS@SO_3H@G-CTS at each stage was higher than that of PS@SO_3H. The first stage below 100 °C was attributed to the loss of physical adsorption water and low-boiling point solvent. The second stage occurring at 150–350 °C was mainly caused by the depolymerization and pyrolysis of chitosan glycosides. The initial stage of chitosan pyrolysis was the random splitting of glycogen bonds, which was further decomposed into acetic acid, butyric acid and some fatty acids. The third stage in the range of 400–500 °C was attributed to the decomposition of polystyrene. In general, the materials exhibited good thermal stability under 200 °C.

3.7 XRD analysis

The XRD spectra of PS, PS@SO_3H and PS@SO_3H@G-CTS were shown in Fig. 7. All three showed a large diffraction dispersion peak at $2\theta = 22.3°$, which was a typical amorphous polystyrene diffraction peak. Compared with PS and PS@SO_3H, there was an obvious diffraction peak at $2\theta = 19.6°$ in PS@SO_3H@G-CTS, attributing to the intramolecular hydrogen bond of chitosan. In

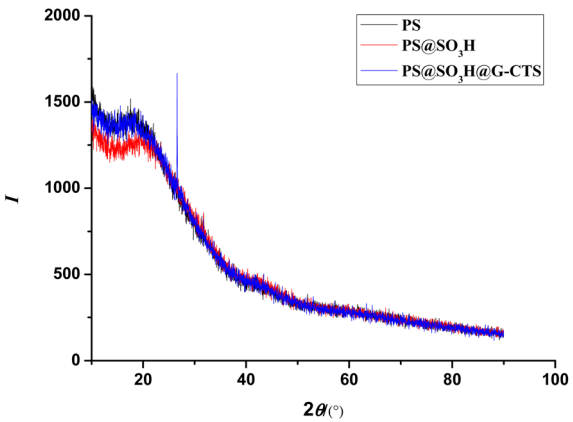

Fig. 7 XRD spectra of PS, PS@SO_3H and PS@SO_3H@G-CTS.

addition, a new peak at $2\theta = 26.6°$ indicated the formation of intermolecular hydrogen bond between the chitosan NH_2 and the sulfonic acid OH on the surface of PS microspheres.

3.8 Comparison of the Pb(II) adsorption

According to the standard curve of Pb(II), the adsorption rates of Pb(II) by PS, CTS, PS@SO_3H and PS@SO_3H@G-CTS were calculated (Fig. 8). Compared with the other three materials, the adsorptivity (102.41%) of PS@SO_3H@G-CTS was the best. Thus, PS@SO_3H@G-CTS was selected as fillers to make SPE column and the desorption of Pb(II) in salt was carried out by standard addition method to evaluate the performance of SPE column.

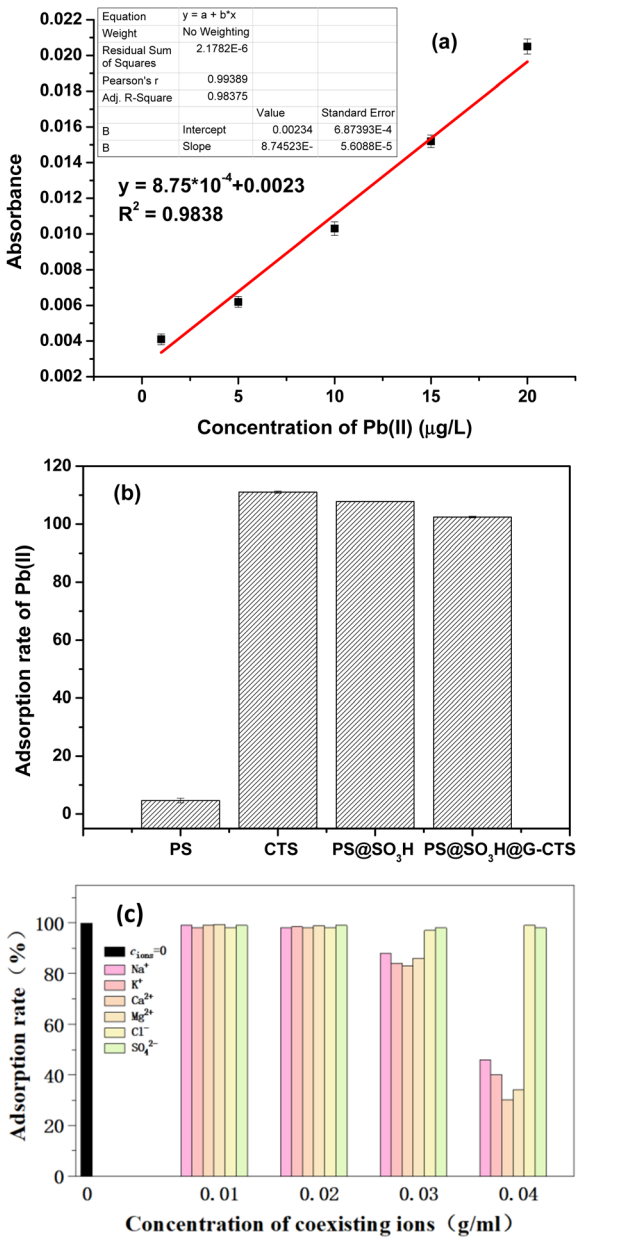

Fig. 8 Adsorbability comparisons for Pb(II) ((a) the standard curve of Pb(II); (b) the adsorption rates of Pb(II) by PS, CTS, PS@SO_3H and PS@SO_3H@G-CTS; (c) anti-interference).

Table 2 Analytical features of PS@SO_3H@G-CTS

LOD (μg L^{-1})	LOQ (μg L^{-1})	Linear range (μg L^{-1})	Relative error (%)
0.08676	0.2892	1–20	0.8579–5.8816

The corresponding analytical features including LOD (limit of detection), LOQ (limit of quantitation), linear range and RSD (relative standard deviation) were shown in Table 2.

Before salt sample analysis, the anti-interference of column in the presence of coexisting cations Na(I), K(I), Ca(II) and Mg(II) as well as anions Cl^- and $SO4^{2-}$ was investigated (Fig. 8c). When the concentration of coexisting ions was lower than 30 g L^{-1}, the adsorption of Pb(II) was not affected. However, when the concentration was increased to 30–40 g L^{-1}, the adsorption of Pb(II) was significantly inhibited with the addition of cations. Among them, the adsorption inhibition caused by Ca(II) and Mg(II) was obviously greater than that caused by Na(I) and K(I). Compared to cations, anions had little effect. So common cations in water will not affect the adsorbability of Pb(II) by SPE column at low concentration, but will significantly inhibit the adsorption with the concentration of more than 40 g L^{-1}. Thus, common anions will not influence the adsorbability of SPE column.

As shown in Fig. 9a, the SPE column exhibited good recovery for Pb(II) with a concentration of salt solution below 0.04 g mL^{-1}. However, with the increase of concentration, especially

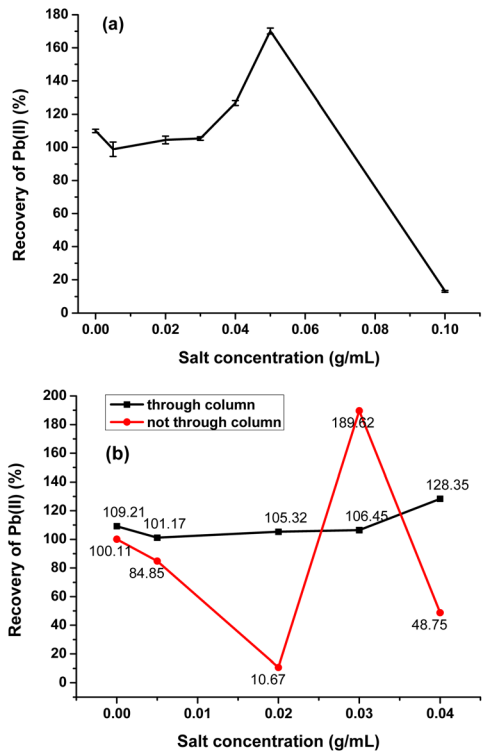

Fig. 9 The adsorption analysis of Pb(II) in real salt sample ((a) the recovery of Pb(II) under different salt concentrations; (b) the comparison of passing and not passing through the column).

above 0.05 g mL^{-1}, the recovery was abnormal and getting lower and lower. In addition, the adsorbability that passing or not passing through the column had obvious difference (Fig. 9b), and the sample passing through the column displayed better and more stable recovery. When the salt concentration was below 0.005 g mL^{-1}, both recoveries of passing and not passing through the column were within normal range, and the recovery of passing through the column was more satisfactory. When the salt concentration was in the range of 0.02 to 0.04 g mL^{-1}, the recovery of not passing through the column became abnormal, but the recovery of passing through the column remained stable, indicating the chitosan-coated PS fillers PS@SO_3H@G-CTS could remove Na(I) efficiently under certain salt condition, so as to accurately detect the heavy metal Pb(II) in the actual sample. The salt concentration not more than 0.03 g mL^{-1} could better reflect the adsorbability of SPE column, with the recovery rate of 101.17–106.45% by standard addition.

Atangana reported formaldehyde-crosslinked chitosan with 13.54% adsorption rate of Pb(II) at the temperature of 25 °C, the pH value of 4, and the adsorption time of 50 min. The method has high requirements for adsorption temperature, time and pH.[38] Hastuti group prepared Pb(II)-imprinted pectin carboxymethyl chitosan with carboxymethyl chitosan as functional monomer, Pb(II) as template ion, and bisphenol A diglycidyl ether as crosslinking agent. It showed obvious selectivity in multiple ions coexistence solution, and the adsorption sequence was Pb(II) > Zn(II). However, the mechanism of molecular imprinting is not yet mature, and the recognition mechanism of molecular imprinted polymers as well as the synthesis of new functional monomers need to be further studied.[39] Compared with the above sorbents, our chitosan-coated polystyrene SPE fillers PS@SO_3H@G-CTS have high removal rate of Pb(II), and the synthetic materials are available and cheap. To especially, the SPE column can be regenerated by using EDTA-2Na solution to wash off the Pb(II). Cost savings, high selectivity and environment-friendliness by recycling could allow PS@SO_3H@G-CTS analysis of Pb(II) in high salt environment.

4. Conclusions

The chitosan-coated polystyrene SPE fillers PS@SO_3H@G-CTS were synthesized *via* chemical bonding with PS microspheres as carrier and glutaraldehyde as crosslinker. The structure was confirmed by elemental analysis, FT-IR, SEM, XRD and thermal stability. It well maintained the surface morphology of PS microspheres, and were easy to separate and collect. The effects of different crosslinkers on the adsorbability of PS@SO_3H@G-CTS were investigated. Chitosan on the surface of PS microspheres could provide effective binding sites for heavy metal Pb(II). The SPE column prepared by PS@SO_3H@G-CTS exhibited excellent adsorbability, anti-interference and recoverability for Pb(II). It was undisturbed by common anions and low concentration of cations. When the salt concentration was less than 0.03 g mL^{-1}, the SPE column could rapidly and effectively adsorb Pb(II). It is very important for instrumental analysis, which can eliminate the influence of high salt matrix, ensure the accuracy of results and avoid equipment loss. Therefore, PS@SO_3H@G-CTS as SPE adsorbents has great potential to analyze heavy metal Pb(II) in high salt environment.

Conflicts of interest

There are no conflicts to declare.

Acknowledgements

This work was supported by the National Key Research and Development Program of China (2018YFC1602800), Natural Science Foundation of Jiangsu Province (BK20211001) of China, and Qing Lan Project (Young Academic Leaders) of Jiangsu Province of China.

References

1 A. Baygan, M. R. A. Mogaddam, F. Lotfipour and M. Nemati, *Int. J. Environ. Anal. Chem.*, 2020, **102**, 1672–1682.
2 A. Chaturvedi, S. Bhattacharjee, V. Kumar and A. K. Singh, *Environ. Sci. Pollut. Res.*, 2021, **28**, 25798–25807.
3 L. Y. Wang, X. L. Peng, H. J. Fu, C. Huang, Y. P. Li and Z. M. Liu, *Biosens. Bioelectron.*, 2020, **147**, 111777.
4 L. R. Bordajandi, G. Gomez, E. Abad, J. Rivera, M. D. Fernandez-Baston, J. Blasco and M. J. Gonzalez, *J. Agric. Food Chem.*, 2004, **52**, 992–1001.
5 C. Reilly, *Metal Contamination of Food: Its Significance for Food Quality and Human Health*, Wiley, Oxford, 3rd edn, 2008.
6 K. S. Ferreira, J. C. Gomes and J. B. P. Chaves, *Food Chem.*, 2005, **92**, 29–32.
7 H. Y. Peng, W. Wang, F. H. Gao, S. Lin, L. Y. Liu, X. Q. Pu, Z. Liu, X. J. Ju, R. Xie and L. Y. Chu, *J. Mater. Chem. C*, 2018, **6**, 11356–11367.
8 H. M. Bao, H. W. Zhang, L. Zhou, H. Fu, G. Q. Liu, Y. Li and W. P. Cai, *ACS Appl. Mater. Interfaces*, 2019, **11**, 28145–28153.
9 S. V. Smirnova, D. V. Ilin and I. V. Pletnev, *Talanta*, 2021, **221**, 121485.
10 A. V. Volzhenin, N. I. Petrova, T. E. Romanova and A. I. Saprykin, *Anal. Lett.*, 2021, **54**, 2293–2303.
11 G. W. Xing, M. R. Sardar, B. X. Lin and J. M. Lin, *Talanta*, 2019, **204**, 50–56.
12 N. Khan, K. Y. Ryu, J. Y. Choi, E. Y. Nho, G. Habte, H. Choi, M. H. Kim, K. S. Park and K. S. Kim, *Food Chem.*, 2015, **169**, 464–470.
13 H. C. Ma, R. An, L. L. Chen, Y. H. Fu, C. Ma, X. L. Dong and X. F. Zhang, *Electrochem. Commun.*, 2015, **57**, 18–21.
14 A. W. Wang, Q. Zhu and Z. P. Xing, *J. Colloid Interface Sci.*, 2019, **555**, 203–213.
15 N. S. Saddam, A. G. Hadi and A. A. Mohammed, *Mater. Today: Proc.*, 2022, **49**, 2793–2796.
16 S. Lombardo, B. Cathala and A. Villares, *Nord. Pulp Pap. Res. J.*, 2021, **36**, 651–661.
17 J. Tong and L. G. Chen, *Anal. Lett.*, 2013, **46**, 2635–2656.
18 Rahmi, Fathurrahmi, Lelifajri and F. Purnama Wati, *Heliyon*, 2019, **5**, e01731.

19 L. L. Fan, C. N. Luo, M. Sun, X. J. Li and H. M. Qiu, *Colloids Surf., B*, 2013, **103**, 523–529.
20 M. A. M. Taguba, D. C. Ong, B. M. B. Ensano, C. C. Kan, N. Grisdanurak, J. J. Yee and M. D. G. de Luna, *Water*, 2021, **13**, 1662.
21 S. Shahraki and H. S. Delarami, *Carbohydr. Polym.*, 2018, **200**, 211–220.
22 S. V. Smirnova, T. O. Samarina, D. V. Ilin and I. V. Pletnev, *Anal. Chem.*, 2018, **90**, 6323–6331.
23 C. Q. Sun, Y. Z. Zhang, Z. S. Gong, X. J. Wang, Y. Yang and Y. Wang, *Int. J. Mass Spectrom.*, 2018, **431**, 22–26.
24 D. Wang, X. G. Chen, J. J. Feng and M. Sun, *J. Chromatogr. A*, 2022, **1675**, 463157.
25 B. Hashemi, P. Zohrabi and M. Shamsipur, *Talanta*, 2018, **187**, 337–347.
26 M. Safari and Y. Yamini, *Talanta*, 2021, **221**, 121648.
27 W. H. Jia, J. Q. Wang, L. M. Ma, S. L. Ren and S. R. Yang, *J. Appl. Polym. Sci.*, 2020, **137**, 48792.
28 M. Ocwieja, D. Lupa and Z. Adamczyk, *Langmuir*, 2019, **34**, 8489–8498.
29 M. Sadowska, Z. Adamczyk and M. Nattich-Rak, *J. Colloid Interface Sci.*, 2017, **505**, 509–518.
30 Y. Y. Liu, J. Y. Zhang, F. G. Tian and Y. Li, *RSC Adv.*, 2020, **10**, 25281.
31 Y. Li, X. j. Wen, X. Y. Ding, X. Teng, X. H. Xiong and Y. Y. Liu, *Res. Chem. Intermed.*, 2022, **48**, 67–83.
32 Y. Y. Liu, Y. Li, L. H. Zong and J. Y. Zhang, *Chem. Res. Chin. Univ.*, 2020, **36**, 781–786.
33 L. Leng, Y. Li and Y. Y. Liu, *Anal. Lett.*, 2017, **50**, 2944–2958.
34 J. Song, C. Q. Zhang, S. W. Kong, F. Y. Liu, W. J. Hu, F. Su and S. M. Li, *Carbohydr. Polym.*, 2022, **291**, 119522.
35 E. S. Singh and T. Singh, *Food Chem.*, 2022, **381**, 132253.
36 V. C. Dumont, I. C. Carvalho, V. B. Andrade, M. A. de Sa, A. J. Ferreira, S. M. Carvalho, A. A. P. Mansur and H. S. Mansur, *Int. J. Polym. Mater. Polym. Biomater.*, 2022, **71**, 740–755.
37 Z. Jahanbakhsh, H. Hosseinzadeh and B. Massoumi, *Polym.-Plast. Technol. Mater.*, 2020, **59**, 1932–1943.
38 E. Atangana, *J. Polym. Environ.*, 2019, **27**, 2281–2291.
39 B. Hastuti, D. Siswanta and M. Triyono, *Bull. Mater. Sci.*, 2019, **42**, 143.